RSC Advances

PAPER

View Article Online
View Journal | View Issue

Cite this: *RSC Adv.*, 2020, **10**, 9063

MOF-derived $ZnCo_2O_4$ porous micro-rice with enhanced electro-catalytic activity for the oxygen evolution reaction and glucose oxidation†

Daojun Zhang, *[ab] Zimo Wang,[a] Jiakai Li,[a] Chengming Hu,[a] Xiaobei Zhang,[b] Bei Jiang,[a] Zhi Cao,[a] Jingchao Zhang[a] and Renchun Zhang[a]

A porous $ZnCo_2O_4$ micro-rice like microstructure was synthesized *via* calcination of a Zn–Co MOF precursor at an appropriate temperature. The as-prepared $ZnCo_2O_4$ sample presented good electrocatalytic oxygen evolution reaction performance with a small overpotential (η_{10} = 389 mV) and high stability in basic electrolyte. Furthermore, in basic medium, the as-synthesized $ZnCo_2O_4$ micro-rice also showed good electrocatalytic activity for glucose oxidation. A $ZnCo_2O_4$ micro-rice modified glass carbon electrode may be used as a potential non-enzymatic glucose sensor. The excellent electrocatalytic OER and glucose oxidation performances of $ZnCo_2O_4$ might be attributed to the unique porous structure formed by the nanoparticles. The porous architecture of the micro-rice can provide a large number of electrocatalytically active sites and high electrochemical surface area (ECSA). The result may offer a new way to prepare low-cost and high performance oxygen evolution reaction and glucose oxidation electrocatalysts.

Received 24th October 2019
Accepted 13th December 2019

DOI: 10.1039/c9ra08723k

rsc.li/rsc-advances

1 Introduction

Metal–organic frameworks (MOFs), also named metal–organic coordination polymers (MOCPs), are a new class of porous materials and have attracted great attention due to their potential applications in the gas storage and separation, catalysis, luminescence, sensing, and energy storage fields.[1–4] In recent years, the micro-nano structured MOFs with special morphologies have been prepared from metal ions and organic ligands in different solvent systems.[5–11] Utilizing MOFs as hard templates or precursors can provide an effective strategy to synthesize novel micro-nano structured materials including metal oxides, metal chalcogenides, metal phosphides, metal carbides, porous carbon materials, and other complex micro-nanostructures.[5–14] The MOF-derived micro-nano materials can exhibit several structure-dependent merits in the electrocatalytic oxygen evolution reaction (OER) and glucose oxidation fields.

In recent years, spinel $A^{II}B_2^{III}O_4$ micro-nano structures have aroused great attention because of their potential application in batteries, supercapacitors, catalytic, and sensing fields.[15] So far, a great of spinel Co_3O_4 ($Co^{II}Co_2^{III}O_4$) structures with different sizes and morphologies have been synthesized as electrode materials for electrochemical oxygen evolution reaction.[16,17] Unfortunately, the Co_3O_4-based electrodes own poor electrical conductivity and high-cost, thus hampered to extensively practical applications. Therefore, using low-cost metal Zn(II) ions to partially substitute Co(II) ions of Co_3O_4 to get $ZnCo_2O_4$ could improve the electrocatalytic properties.[18–20] Ternary $ZnCo_2O_4$ materials reveal higher electrical conductivity and enhanced electrochemical activity ascribed to the co-existence of the Zn and Co species. Therefore, zinc cobalt oxides ($ZnCo_2O_4$) with unique porous structure are anticipated with good performance for electrochemical energy storage and conversion.

Recently, a great of attentions have been paid to the development of electrocatalysts for OER, and OER plays a critical role in water splitting, Zn–air batteries, and regenerative fuel cells fields.[21–27] To date, different Co-based micro-nano structured catalysts, including Co_3O_4,[16,17] Co_3S_4,[28] $CoSe_2$,[29] $CoMoO_4$,[30] Ni_x-$Co_{3-x}(PO_4)_2$,[31] have been developed as OER catalysts and showed good OER performances. On other hand, in recent ten years, electrochemical non-enzymatic glucose sensors based on metal oxides have caused widespread interest due to their easy preparation, cheap cost, and portable characteristics in the detection of glucose.[32–34] Up to now, many metal oxides micro/nano-structures such as NiO, CuO, Co_3O_4, $CuCo_2O_4$, and $NiCo_2O_4$, have been extensively used for glucose sensing.[35–42] Porous hierarchical micro/nano-structures have attracted great interest in electrocatalytic OER and glucose sensing attribute to

[a]*Henan Key Laboratory of New Optoelectronic Functional Materials, College of Chemistry and Chemical Engineering, Anyang Normal University, Anyang 455000, Henan, China. E-mail: zhangdj0410@sohu.com; Tel: +86 372 2900040*

[b]*College of Chemistry and Molecular Engineering, Zhengzhou University, 100 Science Road, Zhengzhou 450001, P. R. China*

† Electronic supplementary information (ESI) available: Size distribution of the Zn–Co-MOF precursor and the calcined sample, the control experiment of Zn–Co-MOF synthesis, TEM images of Zn–Co-based MOF, TG curves, the XPS survey spectrum of $ZnCo_2O_4$. See DOI: 10.1039/c9ra08723k

the unique structure with rich active sites, large electrolyte contact area, and quick electron/active species transfer rate. Based on the above considerations, we exhibit the rational design of $ZnCo_2O_4$ hierarchical porous micro-rice like structure based on thermolysis of a Zn–Co MOF precursor, and the as-prepared material shows enhanced electrocatalytic activity for OER and glucose oxidation.

2 Experimental

2.1 Synthesis of $ZnCo_2O_4$ porous micro-rice like structure

In a typical synthesis procedure, zinc nitrate hexahydrate $Zn(NO_3)_2\cdot 6H_2O$ (0.010 g, 0.03 mmol), cobalt nitrate hexahydrate $Co(NO_3)_2\cdot 6H_2O$ (0.0189 g, 0.06 mmol), *p*-phthalic acid (0.012 g, 0.07 mmol), and polyvinylpyrrolidone (PVP, K30, 0.92 g) were added to the mixture of 5.0 mL *N*-*N*-dimethylformamide (DMF) and 3.0 mL ethanol, the above mixed solution was stirred vigorously for 30 min, sealed and heated to 160 °C for 3 h. After cooling to room temperature, the obtained powder was isolated by centrifugation and washed by ethanol three times, and then dried at 60 °C for 2 h. The porous $ZnCo_2O_4$ micro-rice like structure was obtained by annealing the as-synthesized MOF precursor at 400 °C for 2 h in air (2 °C min^{-1}).

2.2 Reagents and materials characterization

The chemicals include $Zn(NO_3)_2\cdot 6H_2O$, $Co(NO_3)_2\cdot 6H_2O$, glucose (GLU), dopamine (DA), uric acid (UA), ascorbic acid (AA), and polyvinyl pyrrolidone (PVP) were purchased from Beijing Chemical Reagent Co., China. *p*-Phthalic acid was purchased from Aladin Ltd. (Shanghai, China). All of these chemical reagents are of analytical grade and used as received without further purification.

The phase of $ZnCo_2O_4$ was characterized by X-ray diffraction (XRD) on a Rigaku-Ultima III diffractometer with $Cu_{K\alpha}$ radiation. Field scanning electron microscopy (FSEM, Hitachi SU8010) and transmission electron microscopy (TEM, FEI Tecnai G2 s-twin D573) equipments were used to characterize the morphology and microstructure for the as-synthesized samples. The data of specific surface areas was collected by N_2 adsorption on Gemini VII 2390 Analyzer at 77 K. The chemical composition and valence of the obtained materials were analyzed by X-ray photoelectron spectroscopy on XPS Thermo 250Xi. Thermogravimetric analysis (TGA) was carried out in the nitrogen atmosphere on a Netzsch STA-449F3 thermogravimetric analyzer at a heating rate of 10 °C min^{-1}.

2.3 Preparation and measurement of OER electrocatalytic electrode

The electrochemical test was conducted on an electrochemical workstation (CHI 760E) equipped with high-speed rotators from Pine instrument, using O_2 pre-saturated 1.0 M KOH solution as the electrolyte (pH = 14.0). For the electrochemical measurement, a three-electrode setup was employed in which a glassy carbon electrode (GCE) with a diameter of 5 mm (0.196 cm^2), a platinum wire and a Ag/AgCl electrode were employed as the working electrode, counter electrode and reference electrode, respectively. The catalyst ink was prepared as follow, an amount of 5 mg $ZnCo_2O_4$ sample was added to a mixture of H_2O/isopropanol (v/v = 3 : 1, 1 mL) with 50 μL Nafion solution, and the above solution was strongly ultrasonic to acquire a homogenous ink dispersion. Then, 10 μL of the catalyst ink was casted onto the polished GCE and dried at room temperature. The linear sweep voltammetry (LSV) test was carried out with a scan rate of 1 mV s^{-1} at 1600 rpm. Electrochemical impedance spectroscopy (EIS) was recorded at open circuit potential in the frequency scan range from 100 kHz to 0.01 Hz.

2.4 Preparation and measurement of electrochemical sensor electrode

The bare GC electrode was carefully polished with different sizes of Al_2O_3 slurries (1.0, 0.3, and 0.05 μm) prior to modification. The as-obtained $ZnCo_2O_4$ catalyst (1.0 mg) was dispersed to 1.0 mL ultrapure water (18.2 MΩ cm), giving a dispersion with strongly ultrasonic technique. After that, a 5.0 μL of the micro-rice catalysts suspension was dropped on the cleaning GC electrode with a diameter of 3 mm and dried at room temperature before to use.

3 Results and discussion

The scanning electron microscopy (SEM) images of the as-prepared Zn–Co-based MOF precursors and porous $ZnCo_2O_4$

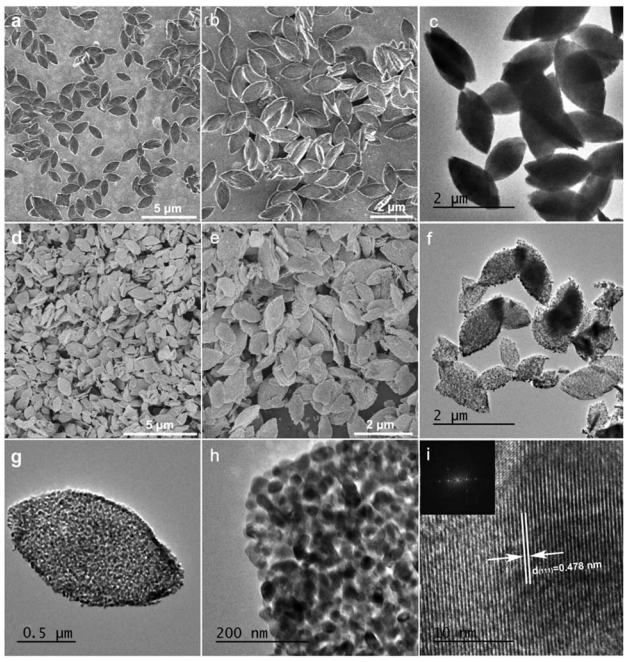

Fig. 1 (a and b) The SEM images of the 3D structure of Zn–Co-based MOF precursors, (c) TEM image of Zn–Co-based MOF precursors, (d and e) the SEM images of the 3D structure of $ZnCo_2O_4$ porous micro-rice like structure obtained after calcination of Zn–Co-based MOF precursors, (f) the TEM image of $ZnCo_2O_4$ porous micro-rice like structure, (g) the TEM image of a single $ZnCo_2O_4$ micro-rice, (h) magnified TEM image of (g), (i) the HRTEM image and FFT of the $ZnCo_2O_4$ porous micro-nano structure (inset).

micro-rice like structure was shown in Fig. 1. The as-prepared MOF precursor displays micro-rice structure roughly 1.71 μm in length and 0.85 μm in width, which assembled by nanosheets (Fig. 1a, b, S1a and b†).

The formation process of the Zn–Co-based MOF precursors was tuned by a series of control experiment. When 0.09 mmol of $Zn(NO_3)_2 \cdot 6H_2O$ was used as raw material with the absence of $Co(NO_3)_2 \cdot 6H_2O$, and kept other reaction parameters unchanged, only microspheres can be obtained. The large size of irregular rectangle-like nanosheets can be obtained when the usage of $Co(NO_3)_2 \cdot 6H_2O$ increased to 0.27 mmol with the Zn/Co molar ratio of 1 : 9 (Fig. S2†). Although most of the micro-rice morphology is remained as decreasing the amount of *p*-phthalic acid to half, however, the dispersibility of nanosheets becomes inferior (Fig. S3†). When tuned the solvent volume ratio of DMF and ethanol from 5 : 3 to 4 : 4, the yield of micro-rice morphology of nanosheets became fewer (Fig. S4†). As shown in Fig. S5,† other things being equal, spindle-like microparticles can be synthesized when DMF was substituted by isometric *N*,*N*-dimethylacetamide (DMA). The TEM image also reveals that a nonporous feature of the precursors and the micro-rice morphology composing of closely stacked lamella with different contrast of the observed layers as shown in Fig. 1c, S6a and b.† Thermogravimetric analysis (TGA) was carried out to evaluate the thermal stability of the Zn–Co MOF sample between 40 and 800 °C. TG curve of MOF shows sharp weight loss of 46.40% from 328 to 399 °C corresponds to the decomposition of the *p*-phthalic acid ligand (Fig. S7†). Thus, we selected 400 °C as the calcination temperature. After annealing at 400 °C for 2 h in atmosphere condition, the MOF precursors can be easily converted to $ZnCo_2O_4$, which maintains the initial micro-rice precursor morphology well with a slight dimension shrinkage (Fig. 1d, e, S8a and b†). The high magnified SEM image in Fig. 1e further demonstrated that the distinctly hierarchical structure of $ZnCo_2O_4$, as shown in the lateral section, which is easy to yield by sintering. The TEM images of $ZnCo_2O_4$ were presented in Fig. 1f and h, clearly certifying porous architecture can be derived from pyrolysis of Zn–Co-based MOF. The porous and hierarchical structure of $ZnCo_2O_4$ with accessible surface facilitated to the fast ions and molecules transfer, suggesting potential good properties. The high resolution TEM image in Fig. 1i indicates the micro-rice presence clear lattice finger with a lattice interplanar space of 0.478 nm, which is corresponded to the (111) crystal plane of spinel $ZnCo_2O_4$. The FFT inset in Fig. 1i also revealed the high crystallinity of the annealed sample.

The XRD pattern of the as-prepared $ZnCo_2O_4$ is shown in Fig. 2a. All the peaks present in the pattern can well match with the standard cards of $ZnCo_2O_4$ (JCPDS 23-1390). Energy-dispersive X-ray (EDX) analysis reveals the coexistence of Zn, Co, O elements in the $ZnCo_2O_4$ micro-rice (Fig. 2b), and the atomic ratio of Zn and Co is about 1 : 2.15. The Brunauer–Emmett–Teller (BET) specific surface area of $ZnCo_2O_4$ obtained from N_2 sorption isotherms is 25 $m^2\ g^{-1}$. The as-synthesized sample shows a typical mesoporous structure with an average pore diameter of ~3.6 nm (inset in Fig. 2c). This unique mesoporous structure is beneficial for molecules/ions diffusion and

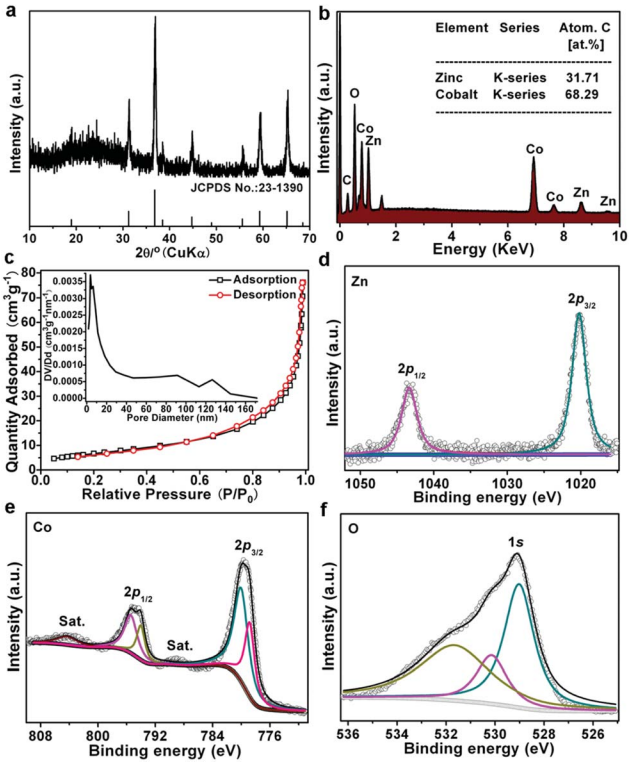

Fig. 2 (a) Powder X-ray diffraction patterns of the simulated and as-synthesized $ZnCo_2O_4$, (b) EDX of the $ZnCo_2O_4$ micro-rice structure, (c) N_2 adsorption/desorption isothermal curve and pore size distribution of the $ZnCo_2O_4$ micro-nano structure, high-resolution XPS spectrum of (d) Zn 2p, (e) Co 2p, (f) O 1s.

adsorption. The surface chemical state of $ZnCo_2O_4$ micro-rice was also investigated by XPS, the survey spectrum in Fig. S5† illustrated the existance of Zn, Co, and O elements. The high-resolution XPS spectrum of Zn 2p in Fig. 2d exhibited two peaks at binding energy of 1020.16 and 1043.40 eV, which is corresponded to Zn $2p_{3/2}$ and Zn $2p_{1/2}$ of Zn^{2+} ions. Meanwhile, the doublet peaks located at 780.16 and 795.42 eV was assigned to Co $2p_{3/2}$ and Co $2p_{1/2}$ of Co^{2+} ions, and another pair of peaks at 778.95 and 794.11 eV was ascribed to Co^{3+} ions (Fig. 2e), which is benefitting for the electrocatalytic process of OER. The O 1s peaks can be deconvoluted into three separated peaks, the peaks of BEs at 529.02 and 531.71 eV matched well with metal–oxygen bonds and physisorption of oxygen in hydroxyl groups, respectively, while, the peak at 530.18 eV suggested the present of oxygen vacancy (Fig. 2f), which could be attributed to the high conductivity of $ZnCo_2O_4$ electrocatalyst.

3.1 OER activity and stability

The OER test of $ZnCo_2O_4$ micro-rice like structure was recorded in an O_2-saturated alkaline solution (1.0 M KOH) with a three-electrode setup. Fig. 3a showed the linear sweep voltammogram (LSV) of catalyst with a scan rate of 1 mV s^{-1}, the overpotential of $ZnCo_2O_4$ micro-rice like structure is 389 mV at current density of 10 mA cm^{-2}, which can compare to some $ZnCo_2O_4$ and Co_3O_4 based catalysts, such as $ZnCo_2O_4$ micro-

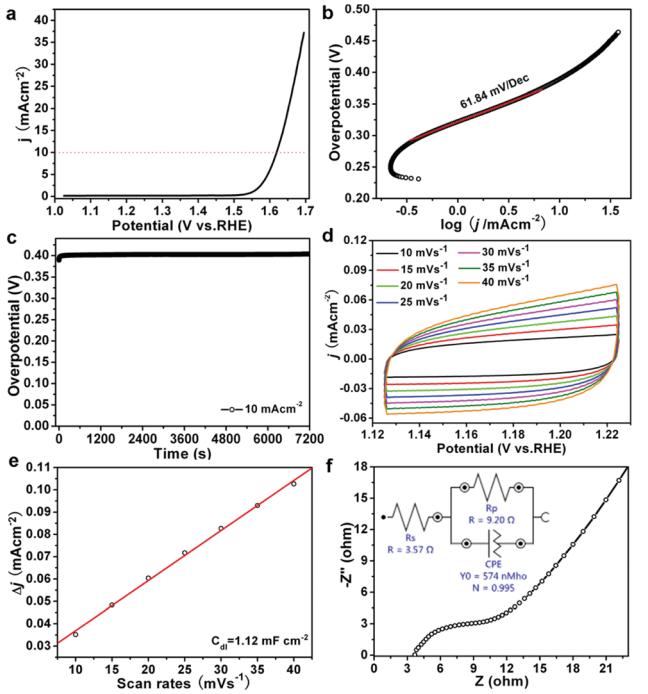

Fig. 3 The catalytic OER process of porous $ZnCo_2O_4$ micro-rice sample: (a) LSV curves obtained at a sweep rate of 1 mV s^{-1}, (b) Tafel plots of OER currents in (a). (c) The chronoamperometry curves at the current density of 10 mA cm^{-2} (d) CVs at different scan rates in 1 M KOH. (e) Plot of current density at 1.17 V (*vs.* RHE) *versus* the scan speed. (f) Nyquist plots of porous $ZnCo_2O_4$ measured at open circuit potential.

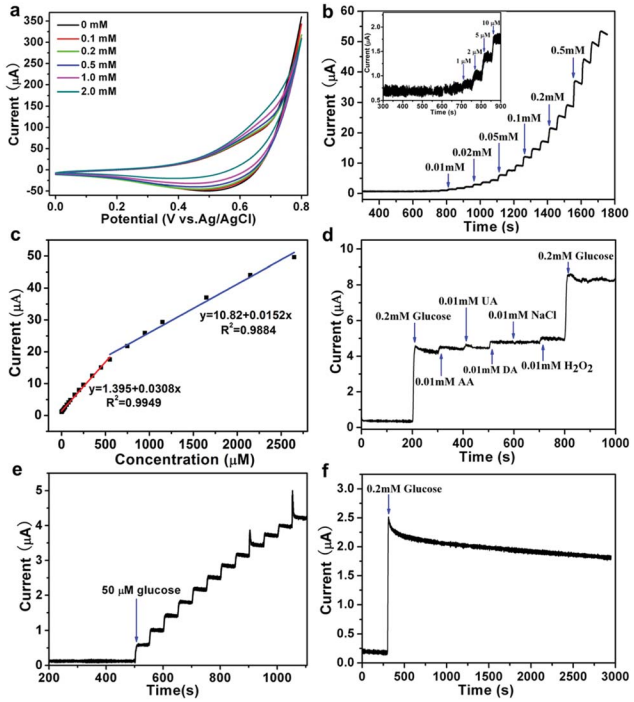

Fig. 4 (a) The CV curves of $ZnCo_2O_4$/GC electrode in the absence and presence of 0.1–2 mM glucose. (b) Amperometric responses of the mesoporous $ZnCo_2O_4$/GC electrode towards successive addition of glucose at the potential of 0.55 V in 0.1 M NaOH. (c) The calibration curve of current response and glucose concentration. (d) The selectivity and anti-interference. (e) The reproducibility of $ZnCo_2O_4$/GC electrode for detection 50 μM glucose. (f) The stability for 2600 s.

spindle,[18] $Zn_{0.3}Co_{2.7}O_4$ porous willow-leaf like structure,[19] mesoporous Co_3O_4,[43] and $CuCo_2O_4$ sample.[44] The Tafel plot of $ZnCo_2O_4$ catalyst was investigated to evaluate the OER performance and as shown in Fig. 3b. The $ZnCo_2O_4$ micro-rice like structure exhibits small Tafel slope of 61.84 mV dec^{-1}. The small Tafel slope of $ZnCo_2O_4$ sample implied a fast OER reaction kinetics and practical applications. Furthermore, stability of the sample was evaluated by chronoamperometry test, as shown in Fig. 3c, the OER overpotential of $ZnCo_2O_4$ micro-rice exhibits almost unchanged during 2 h at the current density of 10 $mAcm^{-2}$, indicating the good durability of the porous sample in alkaline medium. The ECSA of $ZnCo_2O_4$ was evaluated by double-layer capacitance (C_{dl}) and shown in Fig. 3d, the C_{dl} value (1.12 mF cm^{-2}) of $ZnCo_2O_4$ micro-rice structure is not very big (Fig. 3e). The electrochemical impedance spectroscopy (EIS) of $ZnCo_2O_4$ exhibits a small charge transfer resistance of 9.20 Ω (Fig. 3f), revealing that $ZnCo_2O_4$ porous structure own fast charge transfer and small charge transfer resistance for OER process.

3.2 Non-enzymatic glucose sensor

To evaluate the $ZnCo_2O_4$ catalytic performance for nonenzymatic glucose sensing, the CVs was conducted at first. The CV curves of $ZnCo_2O_4$/GC electrodes were recorded in 0.1 M NaOH solution containing 0–2 mM glucose (Fig. 4a), a quick current density response was observed as the increasing of glucose concentration from 0.1–2 mM, which suggested that the porous $ZnCo_2O_4$ modified electrode owns rich active sites for glucose oxidation. Co(II) ions occupy the largest part of the $ZnCo_2O_4$ surface are easily converted to $Co(OH)_2$ in alkaline solution, and the $Co(OH)_2$ can be oxidized to CoOOH intermediate, which can electrocatalytic oxidation the glucose to gluconolactone.

In 0.10 M NaOH solution, the typical amperometric response of the $ZnCo_2O_4$/GC electrode was recorded by the successive addition of glucose at a potential of 0.55 V (Fig. 4b), the modified electrode needs less than 3s to equilibrate each additive amount of glucose. As shown in Fig. 4c, $ZnCo_2O_4$/GC not only showed excellent responds in low detection limit, but also in high concentration, the corresponding calibration curve for glucose detection displayed two linearity regions of 0.01–0.55 mM ($R^2 = 0.9949$) and 0.55–2.65 mM ($R^2 = 0.9884$), and the matched sensitivity of $ZnCo_2O_4$/GC electrode in low and high concentration regions is 436.1 and 215.1 μA mM^{-1} cm^{-2}, respectively. Fig. 4b exhibits the detection limit of $ZnCo_2O_4$/GC electrode is 5 μM, which is lower than CoOOH nanosheet arrays sensor (30.9 μM),[47] Co_3O_4 nanocrystals sensor (50 μM),[49] Co nanobeads/rGO sensor (47.5 μM),[56] octahedral Cu_2O sensor (128 μM),[57] and FeOOH nanowires sensor (15 μM).[59] Both the sensitivity values of the constructed sensor electrode are higher than that of the reported Co_3O_4 porous film electrode (366.03 μA mM^{-1} cm^{-2}),[48] Co_3O_4 nanofibers modified electrode (36.25 μA mM^{-1} cm^{-2}),[52] Co_3O_4/$NiCo_2O_4$ double-shelled nanocages@G

Table 1 Comparison of the performance of the as-prepared $ZnCo_2O_4$ micro-rice sensor with other reported nonenzymatic glucose sensors

Electrode material	Potential (V *vs.* Ag/AgCl)	Linear range (mM)	Detection limit (μM)	Sensitivity (μA mM^{-1} cm^{-2})	Ref.
Cobalt oxide microspheres	+0.55	0.00083–8.61	0.46	669.78	45
Porous CoOOH nanosheet arrays	+0.52	0.003–1.109	1.37	526.8	46
CoOOH nanosheet arrays	+0.40	0.03–0.7	30.9	341.0	47
Co_3O_4 porous film	+0.60	Up to 3.0	1	366.03	48
Co_3O_4 nanocrystals	+0.55	0.1–0.9	50	743.6	49
Co_3O_4 nanowires	+0.20	0.001–1.2	0.265	45.8	50
Nanoporous Co_3O_4 nanowires	+0.60	0.005–0.57	5	300.8	51
Co_3O_4 nanofibers	+0.59	Up to 2.04	0.97	36.25	52
Co_3O_4/$NiCo_2O_4$ double-shelled nanocages@GO	+0.55	0.01–3.54	0.384	304	53
Cobalt oxide NP/r-GO	+0.45 (*vs.* SCE)	0.04–4	1.44	1.21	54
CuO_x–CoO_x/graphene	+0.50 (*vs.* SCE)	0.005–0.57	0.5	507	55
Co nanobeads/rGO	+0.55 (*vs.* SCE)	0.15–6.25	47.5	39.32	56
Octahedral Cu_2O	+0.60	0.3–4.1	128	241	57
CuO microspheres	+0.45 (*vs.* SCE)	0.001–4	0.5	349.6	58
FeOOH nanowires	+0.40 (*vs.* SCE)	0.015–3	15	12.13 (μA mM^{-1})	59
$NiCo_2O_4$ hollow nanorods	+0.60	0.0003–1	0.16	1685.1	60
$ZnCo_2O_4$ microrice	+0.55	0.01–0.55	5	436.1	This work
		0.55–2.65		215.1	

modified electrode (304 μA mM^{-1} cm^{-2}),[53] CuO microspheres modified electrode (349.6 μA mM^{-1} cm^{-2}),[58] CoOOH nanosheet arrays electrode (341 μA mM^{-1} cm^{-2}),[47] and FeOOH nanowires modified electrode (12.13 μA mM^{-1}),[59] but lower than that the $NiCo_2O_4$ hollow nanorods modified electrode with a sensitivity of 1685.1 μA mM^{-1} cm^{-2}.[60] The performance of the as-prepared $ZnCo_2O_4$/GC electrode for glucose sensing is compared with some of recently reported glucose sensors based on Co-based and other transition metal compounds nanomaterials (Table 1).

The selectivity is also a critical factor to assess the performance of an electrochemical sensor. The common existing interferences such as ascorbic acid (AA), uric acid (UA), and dopamine (DA) in human blood serum were researched to evaluate the selectivity of $ZnCo_2O_4$/GC electrode. Fig. 4d shows amperometric response of successive addition of 200 μM glucose, 10 μM AA, UA, DA, 10 μM NaCl, and 200 μM glucose, all the interfering species exhibit negligible responses compared with glucose. The $ZnCo_2O_4$/GC electrode exhibit superior selectivity toward glucose. The reproducibility tested by parallel addition of 50 μM glucose for 12 times, the relative stand deviation is 9.4% (Fig. 4e). The stability of the $ZnCo_2O_4$/GC was tested for 2600 s *via* continuous detection of the amperometric response, and it still retained 72% of the initial value (Fig. 4f). The above results of the $ZnCo_2O_4$/GC electrode demonstrate low detection limit, high sensitivity and good stability for glucose detection, and it may be used as non-enzymatic glucose sensor in the future.

4 Conclusion

A porous $ZnCo_2O_4$ micro-rice like structure was synthesized from a MOF precursor calcinated at a high temperature. The as-prepared $ZnCo_2O_4$ sample presented good electrocatalytic OER activity with a small overpotential (η_{10}) and high stability. The excellent electrocatalytic performance of $ZnCo_2O_4$ may be attributed to the unique porous structure exposed large active sites and high conductivity of $ZnCo_2O_4$. The micro-rice porous structure assembled by nanoparticles can provide many electrocatalytic sites and high ECSA. The result should offer a new designing way to prepare low-cost and high performance electrocatalysts.

Conflicts of interest

There are no conflicts to declare.

Acknowledgements

This work was supported by the National Science Foundation of China (No. 21603004, U1604119, 21501006), the Program for Innovative Research Team of Science and Technology in the University of Henan Province (18IRTSTHN006), and the Natural Science Foundation of Henan Province (182300410194).

Notes and references

1 J. R. Li, Y. G. Ma, M. Colin McCarthy, J. Sculley, J. M. Yu, H.-K. Jeong, P. B. Balbuena and H. C. Zhou, Carbon dioxide capture-related gas adsorption and separation in metal-organic frameworks, *Coord. Chem. Rev.*, 2011, **255**, 1791–1823.
2 Y. B. He, W. Zhou, G. D. Qian and B. L. Chen, Methane storage in metal-organic frameworks, *Chem. Soc. Rev.*, 2014, **43**, 5657–5678.
3 W. P. Lustig, S. Mukherjee, N. D. Rudd, A. V. Desai, J. Li and S. K. Ghosh, Metal- organic frameworks: functional luminescent and photonic materials for sensing applications, *Chem. Soc. Rev.*, 2017, **46**, 3242–3285.

4 Z. B. Liang, C. Qu, W. H. Guo, R. Q. Zou and Q. Xu, Pristine Metal–Organic Frameworks and their Composites for Energy Storage and Conversion, *Adv. Mater.*, 2018, **30**, 1702891.

5 R. R. Salunkhe, Y. V. Kaneti, J. Kim, J. H. Kim and Y. Yamauchi, Nano-architectures for Metal−Organic Framework-Derived Nanoporous Carbons toward Supercapacitor Applications, *Acc. Chem. Res.*, 2016, **49**, 2796–2806.

6 B. Y. Guan, X. Y. Yu, H. B. Wu and X. W. Lou, Complex Nanostructures from Materials based on Metal–Organic Frameworks for Electrochemical Energy Storage and Conversion, *Adv. Mater.*, 2017, **29**, 1703614.

7 A. Indra, T. Song and U. Paik, Metal Organic Framework Derived Materials: Progress and Prospects for the Energy Conversion and Storage, *Adv. Mater.*, 2018, **30**, 1705146.

8 H. Zhang, X. M. Liu, Y. Wu, C. Guan, A. K. Cheetham and J. Wang, MOF-derived nanohybrids for electrocatalysis and energy storage: current status and perspectives, *Chem. Commun.*, 2018, **54**, 5268–5288.

9 H. D. Mai, K. Rafiq and H. Yoo, Nano Metal-Organic Framework-Derived Inorganic Hybrid Nanomaterials: Synthetic Strategies and Applications, *Chem.–Eur. J.*, 2017, **23**, 5631–5651.

10 X. H. Cao, C. L. Tan, M. Sindoro and H. Zhang, Hybrid micro-/nano-structures derived from metal–organic frameworks: preparation and applications in energy storage and conversion, *Chem. Soc. Rev.*, 2017, **46**, 2660–2677.

11 G. Q. Zou, H. S. Hou, P. Ge, Z. D. Huang, G. G. Zhao, D. L. Yin and X. B. Ji, Metal–Organic Framework-Derived Materials for Sodium Energy Storage, *Small*, 2018, **14**, 1702648.

12 S. S. Zhou, C. Hao, J. J. Wang, X. H. Wang and H. W. Gao, Metal-organic framework templated synthesis of porous $NiCo_2O_4/ZnCo_2O_4/Co_3O_4$ hollow polyhedral nanocages and their enhanced pseudocapacitive properties, *Chem.–Eur. J.*, 2018, **351**, 74–84.

13 S. S. Zhou, Z. C. Ye, S. Z. Hu, C. Hao, X. H. Wang, C. X. Huang and F. S. Wu, Designed formation of $Co_3O_4/ZnCo_2O_4/CuO$ hollow polyhedral nanocages derived from zeolitic imidazolate framework-67 for high-performance supercapacitors, *Nanoscale*, 2018, **10**, 15771–15781.

14 C. X. Huang, C. Hao, Z. C. Ye, S. S. Zhou, X. H. Wang, L. L. Zhu and J. B. Wu, In situ growth of ZIF-8-derived ternary $ZnO/ZnCo_2O_4/NiO$ for high performance asymmetric supercapacitors, *Nanoscale*, 2019, **11**, 10114–10128.

15 Q. Zhao, Z. H. Yan, C. C. Chen and J. Chen, Spinels: Controlled Preparation, Oxygen Reduction/Evolution Reaction Application, and Beyond, *Chem. Rev.*, 2017, **117**, 1012–10211.

16 L. Xu, Q. Q. Jiang, Z. H. Xiao, X. Y. Li, J. Huo, S. Y. Wang and L. M. Dai, Plasma-engraved Co_3O_4 nanosheets with oxygen vacancies and high surface area for the oxygen evolution reaction, *Angew. Chem., Int. Ed.*, 2016, **55**, 5277–5281.

17 Y. Li, F. M. Li, X. Y. Meng, S. N. Li, J. H. Zeng and Y. Chen, Ultrathin Co_3O_4 Nanomeshes for the Oxygen Evolution Reaction, *ACS Catal.*, 2018, **8**, 1913–1920.

18 J. C. Zhang, D. J. Zhang, Y. J. Yang, J. Y. Ma, S. F. Cui, Y. M. Li and B. Q. Yuan, Facile synthesis of $ZnCo_2O_4$ mesoporous structures with enhanced electrocatalytic oxygen evolution reaction properties, *RSC Adv.*, 2016, **6**, 92699–92704.

19 J. C. Zhang, B. Q. Yuan, J. Y. Ma, J. J. Wei, J. J. Wang, J. Y. Zhou, R. C. Zhang and D. J. Zhang, Synthesis of $Zn_{0.3}Co_{2.7}O_4$ porous willow-leaf like structure for enhanced electrocatalytic oxygen evolution reaction, *Mater. Lett.*, 2017, **198**, 196–200.

20 Q. H. Wang, L. X. Zhu, L. Q. Sun, Y. C. Liu and L. F. Jiao, Facile synthesis of hierarchical porous $ZnCo_2O_4$ microspheres for high-performance supercapacitors, *J. Mater. Chem. A*, 2015, **3**, 982–985.

21 Y. Jiao, Y. Zheng, M. Jaroniecb and S. Z. Qiao, Design of electrocatalysts for oxygen- and hydrogen-involving energy conversion reactions, *Chem. Soc. Rev.*, 2015, **44**, 2060–2086.

22 W. T. Hong, M. Risch, K. A. Stoerzinger, A. Grimaud, J. Suntivich and Y. Shao- Horn, Toward the rational design of non-precious transition metal oxides for oxygen electrocatalysis, *Energy Environ. Sci.*, 2015, **8**, 1404–1427.

23 J. H. Wang, W. Cui, Q. Liu, Z. C. Xing, A. M. Asiri and X. P. Sun, Recent Progress in Cobalt-Based Heterogeneous Catalysts for Electrochemical Water Splitting, *Adv. Mater.*, 2016, **28**, 215–230.

24 X. X. Zou and Y. Zhang, Noble metal-free hydrogen evolution catalysts for water splitting, *Chem. Soc. Rev.*, 2015, **44**, 5148–5180.

25 Z. L. Wang, D. Xu, J. J. Xu and X. B. Zhang, Oxygen electrocatalysts in metal–air batteries: from aqueous to nonaqueous electrolytes, *Chem. Soc. Rev.*, 2014, **43**, 7746–7786.

26 D. J. Yang, L. J. Zhang, X. C. Yan and X. D. Yao, Recent Progress in Oxygen Electrocatalysts for Zinc–Air Batteries, *Small Methods*, 2017, **1**, 1700209.

27 J. Fu, Z. P. Cano, M. G. Park, A. P. Yu, M. Fowler and Z. W. Chen, Electrically Rechargeable Zinc-Air Batteries: Progress, Challenges, and Perspectives, *Adv. Mater.*, 2017, **29**, 1604685.

28 Y. W. Liu, C. Xiao, M. J. Lyu, Y. Lin, W. Z. Cai, P. C. Huang, W. Tong, Y. M. Zou and Y. Xie, Ultrathin Co_3S_4 nanosheets that synergistically engineer spin states and exposed polyhedra that promote water oxidation under neutral conditions, *Angew. Chem., Int. Ed.*, 2015, **54**, 11231–11235.

29 M. R. Gao, X. Cao, Q. Gao, Y. F. Xu, Y. R. Zheng, J. Jiang and S. H. Yu, Nitrogen-doped graphene supported $CoSe_2$ nanobelt composite catalyst for efficient water oxidation, *ACS Nano*, 2014, **8**, 3970–3978.

30 M. Q. Yu, L. X. Jiang and H. G. Yang, Ultrathin nanosheets constructed $CoMoO_4$ porous flowers with high activity for electrocatalytic oxygen evolution, *Chem. Commun.*, 2015, **51**, 14361–14364.

31 J. C. Zhang, Y. Yang, Z. C. Zhang, X. B. Xu and X. Wang, Rapid synthesis of mesoporous $Ni_xCo_{3-x}(PO_4)_2$ hollow shells showing enhanced electrocatalytic and supercapacitor performance, *J. Mater. Chem. A*, 2014, **2**, 20182–20188.

32 K. Dhara and D. R. Mahapatra, Electrochemical nonenzymatic sensing of glucose using advanced nanomaterials, *Microchim. Acta*, 2018, **185**, 49.
33 G. F. Wang, X. P. He, L. L. Wang, A. X. Gu, Y. Huang, B. Fang, B. Y. Geng and X. J. Zhang, Non-enzymatic electrochemical sensing of glucose, *Microchim. Acta*, 2013, **180**, 161–186.
34 P. Si, Y. J. Huang, T. H. Wang and J. M. Ma, Nanomaterials for electrochemical non-enzymatic glucose biosensors, *RSC Adv.*, 2013, **3**, 3487–3502.
35 F. Y. Xie, X. Q. Cao, F. L. Qu, A. M. Asirie and X. P. Sun, Cobalt nitride nanowire array as an efficient electrochemical sensor for glucose and H_2O_2 detection, *Sens. Actuators, B*, 2018, **255**, 1254–1261.
36 Y. H. Song, C. T. Wei, J. He, X. Li, X. P. Lu and L. Wang, Porous Co nanobeads/rGO nanocomposites derived from rGO/Co-metal organic frameworks for glucose sensing, *Sens. Actuators, B*, 2015, **220**, 1056–1063.
37 L. Wang, Y. L. Zheng, X. P. Lu, Z. Li, L. L. Sun and Y. H. Song, Dendritic copper- cobalt nanostructures/reduced grapheme oxide-chitosan modified glassy carbon electrode for glucose sensing, *Sens. Actuators, B*, 2014, **195**, 1–7.
38 Y. W. Liu, X. Q. Cao, R. M. Kong, G. Du, A. M. Asiri, Q. Lu and X. P. Sun, Cobalt phosphide nanowire array as an effective electrocatalyst for non-enzymatic glucose sensing, *J. Mater. Chem. B*, 2017, **5**, 1901–1904.
39 G. L. Li, H. H. Huo and C. L. Xu, $Ni_{0.31}Co_{0.69}S_2$ nanoparticles uniformly anchored on a porous reduced graphene oxide framework for a high-performance non- enzymatic glucose sensor, *J. Mater. Chem. A*, 2015, **3**, 4922–4930.
40 Y. Shu, B. Li, J. Y. Chen, Q. Xu, H. Pang and X. Y. Hu, Facile Synthesis of Ultrathin Nickel−Cobalt Phosphate 2D Nanosheets with Enhanced Electrocatalytic Activity for Glucose Oxidation, *ACS Appl. Mater. Interfaces*, 2018, **10**, 2360–2367.
41 Y. Y. Su, B. B. Luo and J. Z. Zhang, Controllable Cobalt Oxide/Au Hierarchically Nanostructured Electrode for Nonenzymatic Glucose Sensing, *Anal. Chem.*, 2016, **88**, 1617–1624.
42 W. Huang, Y. Cao, Y. Chen, J. Peng, X. Y. Lai and J. C. Tu, Fast synthesis of porous $NiCo_2O_4$ hollow nanospheres for a high-sensitivity non-enzymatic glucose sensor, *Appl. Surf. Sci.*, 2017, **396**, 804–811.
43 Y. J. Sa, K. Kwon, J. Y. Cheon, F. Kleitzc and S. H. Joo, Ordered Mesoporous Co_3O_4 Spinels as Stable, Bifunctional, Noble Metal-Free Oxygen Electrocatalysts, *J. Mater. Chem. A*, 2013, **1**, 9992–10001.
44 Y. K. Zhao, X. C. Zhou, Y. Ding, J. W. Huang, M. Zheng and W. C. Ye, A study of photocatalytic, chemical, and electrocatalytic water oxidation on ACo_2O_4 (A = Ni, Cu, Zn) samples through doping different metal ions, *J. Catal.*, 2016, **338**, 30–37.
45 S. Q. Ci, S. Mao, T. Z. Huang, Z. H. Wen, D. A. Steeber and J. H. Chen, Enzymeless Glucose Detection Based on CoO/Graphene Microsphere Hybrids, *Electroanal*, 2014, **26**, 1326–1334.
46 L. Zhang, C. L. Yang, G. Y. Zhao, J. S. Mu and Y. Wang, Self-supported porous CoOOH nanosheet arrays as a non-enzymatic glucose sensor with good reproducibility, *Sens. Actuators, B*, 2015, **210**, 190–196.
47 K. K. Lee, P. Y. Loh, C. H. Sow and W. S. Chin, CoOOH nanosheets on cobalt substrate as a non-enzymatic glucose sensor, *Electrochem. Commun.*, 2012, **20**, 128–132.
48 S. S. Fan, M. G. Zhao, L. J. Ding, J. J. Liang, J. Chen, Y. C. Li and S. G. Chen, Synthesis of 3D hierarchical porous Co_3O_4 film by eggshell membrane for non-enzymatic glucose detection, *J. Electroanal. Chem.*, 2016, **775**, 52–57.
49 M. Li, C. Han, Y. F. Zhang, X. J. Bo and L. P. Guo, Facile synthesis of ultrafine Co_3O_4 nanocrystals embedded carbon matrices with specific skeletal structures as efficient non-enzymatic glucose sensors, *Anal. Chim. Acta*, 2015, **861**, 25–35.
50 K. Khuna, Z. H. Ibupoto, X. Liu, V. Beni and M. Willander, The ethylene glycol template assisted hydrothermal synthesis of Co_3O_4 nanowires; structural characterization and their application as glucose non-enzymatic sensor, *Mater. Sci. Eng., B*, 2015, **194**, 94–100.
51 L. Q. Kang, D. P. He, L. L. Bie and P. Jiang, Nanoporous cobalt oxide nanowires for non-enzymatic electrochemical glucose detection, *Sens. Actuators, B*, 2015, **220**, 888–894.
52 Y. Ding, Y. Wang, L. Su, M. Bellagamba, H. Zhang and Y. Lei, Electrospun Co_3O_4 nanofibers for sensitive and selective glucose detection, *Biosens. Bioelectron.*, 2010, **26**, 542–548.
53 B. Xue, K. Z. Li, L. Feng, J. H. Lu and L. L. Zhang, Graphene wrapped porous $Co_3O_4/NiCo_2O_4$ double-shelled nanocages with enhanced electrocatalytic performance for glucose sensor, *Electrochim. Acta*, 2017, **239**, 36–44.
54 H. Heidari and E. Habibi, Amperometric enzyme-free glucose sensor based on the use of a reduced graphene oxide paste electrode modified with electrodeposited cobalt oxide nanoparticles, *Microchim. Acta*, 2016, **183**, 2259–2266.
55 S. J. Li, L. L. Hou, B. Q. Yuan, M. Z. Chang, Y. Ma and J. M. Du, Enzyme-free glucose sensor using a glassy carbon electrode modified with reduced graphene oxide decorated with mixed copper and cobalt oxides, *Microchim. Acta*, 2016, **183**, 1813–1821.
56 Y. H. Song, C. T. Wei, J. He, X. Li, X. P. Lu and L. Wang, Porous Co nanobeads/rGO nanocomposites derived from rGO/Co-metal organic frameworks for glucose sensing, *Sens. Actuators, B*, 2015, **220**, 1056–1063.
57 Y. C. Li, Y. M. Zhong, Y. Y. Zhang, W. Weng and S. X. Li, Carbon quantumdots/octahedral Cu2O nanocomposites for non-enzymatic glucose and hydrogen peroxide amperometric sensor, *Sens. Actuators, B*, 2015, **206**, 735–743.
58 X. D. Liu, Y. Yang, R. Y. Liu, Z. L. Shi, L. Y. Ma and M. Wei, Synthesis of porous CuO microspheres assembled from (001) facet exposed nanocrystals with excellent glucose-sensing performance, *J. Alloys Compd.*, 2017, **718**, 304–310.
59 C. Xia and W. Ning, A novel non-enzymatic electrochemical glucose sensor modified with FeOOH nanowire, *Electrochem. Commun.*, 2010, **12**, 1581–1584.
60 J. Yang, M. Cho and Y. Lee, Synthesis of hierarchical $NiCo_2O_4$ hollow nanorods *via* sacrificial-template accelerate hydrolysis for electrochemical glucose oxidation, *Biosens. Bioelectron.*, 2016, **75**, 15–22.